Journal of Drug Delivery Science and Technology 99 (2024) 105978

Contents lists available at ScienceDirect

Journal of Drug Delivery Science and Technology

journal homepage: www.elsevier.com/locate/jddst

The airflow and the regional particle behavior in a human airway under the circulatory breathing conditions: A numerical study

Dogan Ciloglu

Department of Mechanical Engineering, Ataturk University, 25240, Erzurum, Turkey

ARTICLE INFO

Keywords:
Pulmonary airflow dynamics
Circulatory breathing
Aerosol particle
Regional deposition
Computational fluid dynamics

ABSTRACT

Inhalation therapy is one of the methods for treating pulmonary diseases such as asthma, chronic obstructive pulmonary disease, and lung infections. Thus, prediction of local deposition of inhaled particles is crucial for the assessment of their therapeutic effects. However, there are limited studies that performed under realistic respiratory conditions, especially with respect to targeted drug delivery. The main goal of this study is to numerically investigate the regional transport and deposition of the aerosol particles in a realistic human airway model during the circulatory breathing conditions. In the simulations, three different circulatory breathing conditions and the aerosol particle sizes were conducted. Results obtained from simulations suggest that the distribution and deposition of the particles were significantly affected by the inhalation flow rate, the particle size, and the type of breathing conditions. The particle deposition efficiencies increased with flow rate and particle size. Most of particles deposited in the extrathoracic region before reaching the bronchial region. It is advisable to avoid selecting a high inhalation flow rate for the effective treatment of bronchial diseases. Both the particle distribution fraction and the deposition efficiency were higher in the right lung compared to the left lung. Thus, it can be said that the right lung will absorb more drugs and be more effective in treating the diseases. For the treatment of the left lung diseases, the inhalation flow rate should be increased appropriately. However, it should not be forgotten that this situation can increase a possible health risk by inhaling pollutants in the air.

1. Introduction

An effective way for therapeutic drug delivery in the human respiratory tract is the inhalation of aerosol particles. This approach improves the drug's delivery efficiency to the intended location, resulting in a substantial reduction of potential side effects associated with the drug [1–3]. Although inhaler devices are designed to deliver aerosol particles through the respiratory airways, not all the particles inhaled reach the targeted areas due to several key factors including the airway geometry, breathing pattern, and particle properties [4–6]. In this case, the patient may be exposed to potential side effects and inappropriate treatment. To tackle this challenge, a comprehensive examination of how inhaled particles interact within the human respiratory tract is essential.

The human respiratory system including the extrathoracic (nose, mouth, pharynx, and larynx), conducting (generations 0–16), and alveolar airways (generations 17–23) has a complex structure with successive bifurcations. Assessing airflow and particle dynamics in such a complex structure is quite challenging due to the constraints of existing imaging technologies, the unique morphology of patient-specific lung, variations in airway geometry during respiration, as well as the costs and the potential risks associated with *in vivo* experiments [7]. On the other hand, determining the airflow using *in vitro* experimental methods on a 3D airway model with a realistic and complex structure is both costly and long-run time. Therefore, the computational fluid dynamics (CFD) based *in silico* modeling has recently been widely used to analysis and provide such knowledge in all respiratory conditions [4,8–11]. In this context, the transport equations governing the airflow, particle transport, and deposition in the human respiratory airways are solved, assuming laminar or turbulent flow depending on the initial flow conditions. Many researchers have utilized the airway models based on the non-realistic (Weibel A model) and realistic (computed tomography (CT)-based) lung models [12–20]. The common feature of all idealized models, such as the Weibel's model [21], is a significant simplification of the real lung geometry by ignoring surface irregularities, physiological features, protrusions, and surface roughness. Many numerical and experimental studies on the airflow in the respiratory tract have traditionally utilized simplified and idealized airway models derived from such early morphological studies. Thanks to thoracic CT images, the

E-mail address: dciloglu@atauni.edu.tr.

https://doi.org/10.1016/j.jddst.2024.105978
Received 26 February 2024; Received in revised form 19 June 2024; Accepted 14 July 2024
Available online 17 July 2024
1773-2247/© 2024 Elsevier B.V. All rights are reserved, including those for text and data mining, AI training, and similar technologies.

human airway models can now be constructed more realistically without the need for certain assumptions in the idealized models, thus enabling more accurate prediction of inhaled particle behavior nowadays [16].

Fleming et al. [22] utilized 3D radionuclide imaging with CT scanning of the airways to provide a more comprehensive report on the deposition zones of aerosols within the respiratory tract. Golshahi et al. [23] found intriguing results by measuring the deposition of microparticles (0.5 and 5.3 μm) in replicas of older children (aged 4 and 14 years). Their aimed was to establish correlations between the morphological features of the airways and breathing conditions, which could serve as a predictive tool for potential future enhancements in environmental and pharmaceutical standards. Rahimi-Gorji et al. [16–24] conducted two-phase flow simulations using multiple inhalation flow rates (10–60 L/min) on a CT-based realistic tracheobronchial airway model. The results showed that aerosol particle deposition strongly depends on the aerodynamic particle diameter. Moreover, particle deposition increased with increasing flow rate, and inertial impaction played a dominant role in upper bronchial airways. Ahookhosh et al. [18] used an airway model generated by rapid prototyping techniques with the help of CT data from a healthy 48-year-old woman, extending from the oral cavity to the fourth generation of the tracheobronchial tree. They experimentally investigated the differences between a dry powder inhaler (DPI) and a metered dose inhaler (MDI) using this model. Ciloglu and Karaman [25] numerically examined the airflow and the aerosol particle dynamics on a realistic airway model under multiple steady-state breathing cycles. They stated that the deposition fractions increased with increasing particle size and flow rate, and inertial impaction affected particle deposition. Poorbahrami and Oakes [26] examined the impact of specific anatomical features on airflow and particle distributions by modeling three subject-specific airway geometries. They reported that total particle deposition percentages ranged from 3 % ($d_p = 5$ μm) to 20 % ($d_p = 1$ μm) between subjects, and the flow characteristics affected the local particle deposition. Their simulations provide the first overview of both localized and global deposition variability. Ahookhosh et al. [27] conducted a study on the transport and deposition of microparticles in human respiratory system using pressurized metered-dose inhalers for drug delivery. Their findings revealed that particle deposition in the right bronchus was higher than in the left bronchus. A similar paper by Ahookhosh et al. [28] studied the airflow and the particle deposition under different breathing flow rates in a patient specific airways model consisting of the extrathoracic and tracheobronchial regions up to the 5th airway generation. Their results showed that when respiratory flow rates increased, particles tended to accumulate more in the model due to vortex effects. Calmet et al. [29] investigated the dynamic behavior of airflow and the transport of inhaled aerosols in a realistic human upper airway geometry during sniffing. Koullapis et al. [30] observed that substantial differences in the flow field below the main bifurcation were absent. The variations in local particle deposition were predominantly attributed to variances in the mouth-throat filtration, as opposed to upstream effects or differences in local flow field.

In many previous numerical studies using realistic models, the airflow field in the human airways has been considered with the assumption of the inhalation airflow at a constant speed. Ostrovski et al. [31] conducted a numerical study focusing on the specific distribution of aerosols in the proximal zones of the upper respiratory tract. They used a steady-state flow rate of 3 L/min in their simulations. Their findings showed that unlike particles smaller than 2 μm, the particles in the 5–10 μm range were most effective for deposition in the upper respiratory tract, with deposition fractions ranging from 0.68 to 1. Xu et al. [32] examined airflow in the trachea using the particle image velocimetry (PIV) and the CFD techniques in a realistic human airway model. The authors applied constant airflow rates of 36 L/min, 64 L/min, and 90 L/min during inhalation and exhalation. They stated that as flow velocities increased, the glottal jet phenomenon became less pronounced, and the area of the separation zone became smaller. In another study, Arsalanloo et al. [33] investigated the transport and deposition of particles under the constant breathing conditions of 15, 30, and 60 L/min in a realistic model based on CT-scan images of a healthy 28-year-old male. The results indicated that most particles are directed towards the right lung, although the left lung demonstrates a higher rate of deposition efficiency. Wang et al. [34] conducted the simulations to predict the behavior of airflow and drug particles in a patient-specific 3D tracheobronchial geometry, spanning from the trachea to the sixth generation in patients experiencing COVID-19 symptoms. The airflow and the trajectory of the particles were numerically resolved at a steady-state breathing rate of 15 L/min. Their findings suggest that segment-specific targeted drug therapy delivery was viable. Consequently, a detailed analysis of airflow and aerosol particle dynamics in the respiratory airways is needed for effective inhaled drug therapy. This is particularly important for patients with lung disease and those who have undergone surgical reconstruction or intervention in their airways.

In the above-mentioned studies, most researchers have either focused on specific regions of the human respiratory system or have used the assumption of steady-stead airflow conditions. Indeed, the aerosol particle deposition is mainly observed under normal breathing conditions. However, the airflow field characteristics and the aerosol deposition in a realistic human airway model during circulatory breathing have rarely been investigated. In the upper regions of the lung airways, especially in the mouth, pharyngeal, and extrathoracic airways, airflow and particle behaviors play a crucial role in delivering drug particles to the deep lung. The primary objective of this study is to examine the regional transport and deposition of aerosol particles of various microsizes through *in silico* assessment under the realistic breathing conditions. In the simulations, a CT based model of the human airway including the mouth-throat region and the tracheobronchial upper respiratory tract was used. A one-way coupled Lagrangian method was also applied to track the trajectories of aerosol particles and simulate their deposition. Three circulatory breathing conditions representing light, normal, and heavy activities were employed and the results were compared to those of constant breathing conditions.

2. Materials and method

2.1. Construction of anatomical model and mesh generation

A 3D anatomical model of the mouth-throat area and the tracheobronchial upper lung airways has been created based on digital CT scans of a 37-year-old healthy male, provided by the Ataturk University Research Hospital, Erzurum, Turkey. The resulting human airways is reconstructed by the SolidWorks software as in the author's previous work [25]. Prior to creating the mesh structure for numerical simulations, a smoothed geometry is obtained by making some geometric arrangements on the anatomical model such as thresholding, mask modification, and part calculation. In order to report the regional depositions, then, the whole model divided into different segments by the physiological structure. Fig. 1 shows the simulated structure of the human airways in this study, involving the names and locations of various segments. The morphological features of the model, such as diameter, length, surface area, and volume of the distinct segments, are detailed in Table 1. After that, the model domain is meshed into tetrahedral elements by ANSYS Fluent Meshing (Fluent 19.0, ANSYS Inc., Canonsburg, PA). To ensure proper simulation of flow in the boundary layer region adjacent to the model walls, ten-layer inflation is conducted near the wall. The various views of the generated mesh are illustrated in Fig. 2.

In order to determine the optimum state where the results do not change considerably with more refinement of the mesh, the mesh independency analysis must be carried out before the numerical simulations. Six different meshes sizes with the cell numbers of 0.9 million (Mesh-1), 1.02 million (Mesh-2), 1.37 million (Mesh-3), 1.85 million

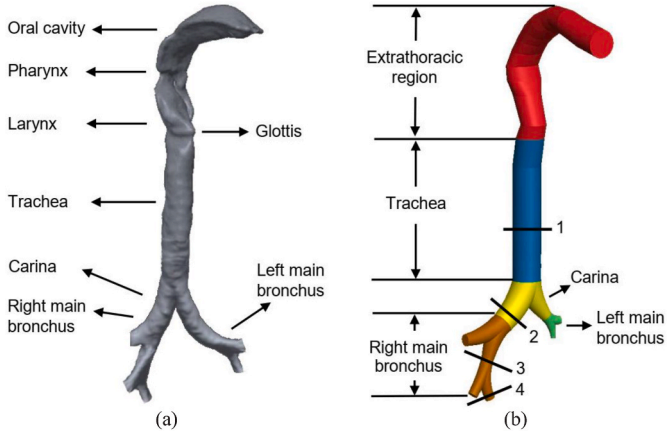

Fig. 1. The 3D geometry of (a) the realistic model and (b) the segments of reconstructed human airway model.

Table 1
Geometric parameters of the present model.

Segments	Diameter (cm)	Length (cm)	Surface area (cm^2)	Volume (cm^3)
Oral cavity	2	6.09	37.19	17.91
Pharynx	2.26	5.18	39.37	20.07
Larynx	2.11	6.06	38.98	18.28
Trachea (G0)	2	8	50.2	25.07
Right G1	15.6	35	20.59	8.53
Right G2	8.3	33.1	14.93	3.81
Right G3	7.1	27.63	6.66	1.36
Left G1	8.3	31	543	2.49
Left G2	5.9	12.4	1.16	0.22
Left G3	2.95	17.71	3.77	0.47

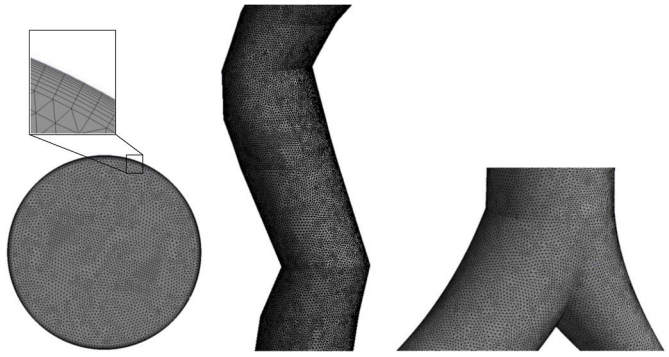

Fig. 2. Various views of the generated mesh. (a) Oral inlet, (b) Pharynx-Larynx part, and (c) Bronchus.

(Mesh-4), 2.45 million (Mesh-5) and 3,85 million (Mesh-6) have been used in this study. Fig. 3 illustrates the mesh refinement results depend on dimensionless velocity profiles and pressure on line 1 (see Fig. 1b). It can be seen that the results do not change significantly with the increase in the number of elements from 1.85 million to 2.45 million. Therefore, Mesh-5 has been selected for all numerical simulations.

2.2. Airflow modeling

The airflow within the generated human airways model is solved using Fluent 19.0. The nature of the respiration process is unsteady, and for this study, the oscillatory flow conditions are employed. In this regard, the fluid flow is numerically simulated by solving the time-dependent 3D Navier-Stokes equations for the incompressible flow:

$$\frac{\partial u_i}{\partial x_i} = 0 \tag{1}$$

$$\frac{\partial u_i}{\partial t} + u_j\frac{\partial u_j}{\partial x_j} = -\frac{1}{\rho}\frac{\partial p}{\partial x_i} + \frac{\partial}{\partial x_j}\left[(\nu + \nu_T)\left(\frac{\partial u_i}{\partial x_j} + \frac{\partial u_j}{\partial x_i}\right)\right] \tag{2}$$

where u_i, u_j denotes the velocity components in x, y and z direction, p is the air pressure, ρ is the air density, ν is the kinematic viscosity, and ν_T is the turbulent viscosity.

2.3. Boundary conditions

In this study, the k-ω turbulence model has been utilized to capture airflow due to its higher accuracy and superior adaptability to modeling internal fluxes compared to the k-ε model [35–37]. Three sinusoidal peak flow rates of 15, 30, and 60 L/min have been implemented to simulate the breathing conditions associated to light, normal and heavy activity, respectively. The area of the mouth inlet is 0.314×10^{-3} m^2, so the average velocities corresponding to each flow rate are approximately 0.79, 1.59, and 3.18 m/s, respectively. A sinusoidal breathing waveform is used as $q(t) = A.\sin(\omega t)$, where A is the respective peak flow rates and ω is the circular frequency. The actual breathing airflow waveform is not exactly sinusoidal. However, studies have shown that there is no significant difference between the actual and the circulatory breathing airflow profiles. Therefore, the three respiratory conditions used in this study can be approximated through a sinusoidal waveform [38–40]. The parameters are set so that the breathing profile provided a tidal volume of 500 mL during 2 s inspiration and 2 s expiration (i.e., 15 normal breaths per minute). The waveforms and Reynolds numbers at the inlet of circulatory breathing are depicted in Fig. 4.

The governing equations are solved by utilizing a pressure-based and implicit solver with the Least-squares cell-based gradient option for each transient breathing cycle. In these simulations, the Coupled method, the PRESTO discretization scheme, and the second-order upwind scheme are applied for pressure-velocity coupling, pressure, and momentum, respectively. A uniform distributed velocity is imposed at the mouth inlet and a zero gauged pressure condition is maintained at all the outlets of the airway model, which correspond to the ends of the third-generation bronchi. The model' walls are considered stationary, and the no-slip boundary condition is applied at the wall boundaries. Furthermore, the fluid properties of the air at 20 °C are considered. In the numerical simulations, the time step has been taken as 0.05 s. It is assumed that the problem has converged when the residuals reduced below 10^{-6}.

2.4. Particle transport modeling

In order to simulate the trajectories and deposition of the aerosol particles in the computational domain, the Eulerian-Lagrangian approach is applied. Because the Brownian force is significant in the laminar flow and for the sub-micron particles [41], its effect in this simulation is also negligible. Hence, the equations of motion including the primary forces on particles such as the drag and the gravitational forces is written as:

$$m_p\frac{d\vec{u}_p}{dt} = \vec{F}_D + \vec{F}_G \tag{3}$$

where $\vec{F}_D$ and $\vec{F}_G$ are the drag and the gravitational forces, respectively. For the spherical particles, $\vec{F}_D$ is defined as:

$$\vec{F}_D = \frac{1}{2}C_D A_p\left(\vec{u} - \vec{u}_p\right)\left|\vec{u} - \vec{u}_p\right| \tag{4}$$

where C_D is the drag force coefficient given by:

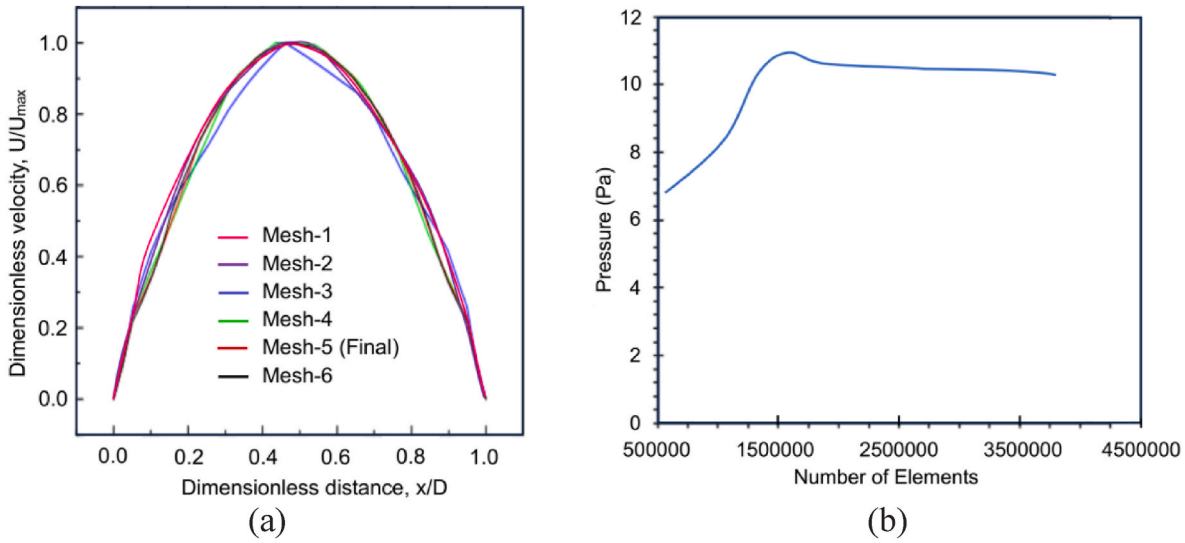

Fig. 3. Comparison of (a) the velocity profiles on line 1 for mesh-independent test and (b) total pressure as functions of grid number at the flow rate 30 L/min.

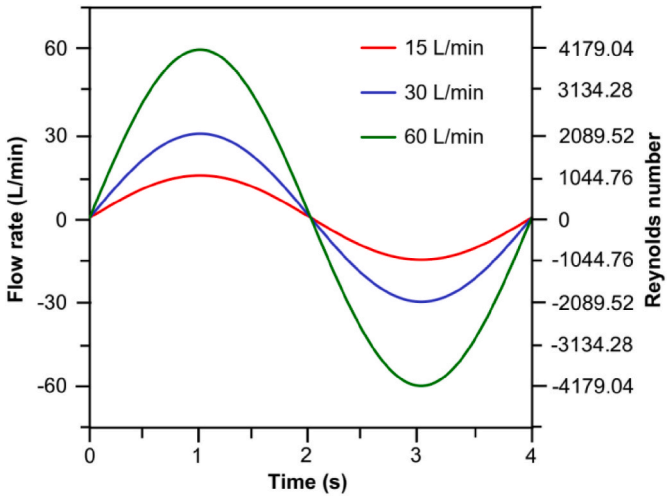

Fig. 4. The inhalation flow waveforms and Reynolds number.

$$C_D = a_1 + \frac{a_2}{Re_p} + \frac{a_3}{Re_p^2} \tag{5}$$

where a_1, a_2, and a_3 are constants proposed by Morsi and Alexander [42]. The particle Reynolds number is:

$$Re_p = \rho \left| \vec{u} - \vec{u}_p \right| d_p \Big/ \mu \tag{6}$$

$\vec{F}_G$ is expressed as:

$$\vec{F}_G = m_p(\rho_p - \rho)\frac{\vec{g}}{\rho_p} \tag{7}$$

where $\vec{g}$ is the gravitational acceleration vector, pointing in the negative z-direction in this study.

In the numerical simulations, 60,000 spherical particles with a uniform diameter were randomly injected from the mouth inlet with the same velocity of the air. This particular particle number provided the deposition results independent of the number of particles released. In order to simulate the typical aerosol particles, the particles were selected with a density of 1100 kg/m^3 and three different aerodynamic diameters (2, 5 and 7 μm) [14,24]. The "trap" and "escape" conditions are implemented on the airway walls for particles deposition and the outlets, respectively [43]. It can be said that the 'trap' condition is suitable due to the mucus layer present in the inner surfaces of airway walls. Therefore, during the breathing cycles, the aerosol particles get trapped on the inner surface of the lungs, exit the specific zone, or remain suspended in the suspension, instead of bouncing back. A one-way coupling model was applied in the simulations, assuming that the particulate phase has a negligible effect on the surrounding fluid phase. In addition, the particle aggregation during their transportation and deposition into the human lung is not considered. The particle deposition fraction (DF) and the regional deposition efficiency (η_d) of the aerosol particles in the human airways is calculated as, respectively;

$$DF = \frac{number\ of\ deposited\ particles\ in\ a\ specific\ region}{number\ of\ particles\ entering\ the\ mouth} \tag{8}$$

$$\eta_d = \frac{number\ of\ deposited\ particles\ in\ a\ specific\ region}{number\ of\ particles\ entering\ this\ region} \tag{9}$$

Two subsequent breath cycles (8 s of total breathing cycle) were applied in the simulations. To eliminate the perturbation effect, only air was provided during the first breathing cycle. The particle release into the computational domain was started at the beginning of the second breathing cycle (t = 4 s) and stopped at its end (t = 6 s). As a result, their trajectories within the computational domain were tracked using the Lagrangian method during two breathing cycles. The particles in contact with the airway wall were considered as deposited due to the presence of the mucus layer. It was also supposed that particles reaching the outlets of different lung lobes move towards deeper airways by leaving the computational domain. Suspended particles were tracked again during exhalation, and the particles that completely exited the airway model were disregarded.

3. Results and discussion

3.1. Model validation

In this study, the validation of airflow and particle deposition in the human airways is provided by considering the G0-G3 generations and flow rates ranging from 15 to 120 L/min. In order to validate the present simulation, the results were compared with the reported in previous studies. Borojeni et al. [44] used a correlation developed by Chan and Lippmann [45] to examine aerosol dynamics in the upper respiratory tract and was effective in determining the overall deposition efficiency

in adult human subjects. The correlation was dependent only on the Stokes number in each lung airway generation. The data obtained using this correlation was compared to our model prediction. Similarly, Cheng et al. [46] examined the particle size effects and the airflow rate on particle deposition in the mouth, pharynx, larynx, trachea, and 3-generation airway model. In their study, the researchers used constant flow rates of 15, 30, and 60 LPM to examine the local deposition of aerosol particles of nine different sizes in a human airway replica, and the DE against the impaction and the Stokes number were investigated. Hofmann et al. [47] evaluated the effects of physical activity levels on particle deposition in an adult human. Schlesinger et al. [48] reported the deposition of aerosols with aerodynamic diameters ranging from 2.5 to 8.1 mm at three different inspiratory flow rates in a model including the larynx and tracheobronchial tree. The deposition efficiency of particles as a function of impaction parameter for particles is presented in Fig. 5. As shown in Fig. 5, there is a good agreement between the current results and previous studies, indicating the validity of the current numerical method. The reason for the incomplete overlap in deposition efficiencies can be explained by the variation between the analyzed geometries, as well as the experimental conditions and the different numerical methods employed in each study.

3.2. Airflow characteristics

The complex morphological structure of the human respiratory tract can significantly influence its flow characteristics. This affects the flow streamlines and causes the secondary flows to form, resulting in the asymmetric flow. All these factors alter the local pattern of particle deposition in different regions and thus, it is important to investigate the flow patterns and the characteristics in different regions of the human respiratory system. For a given inhalation flow rate, the velocity contours at any time during inhalation (e.g., between 1 and 2 s) and exhalation (e.g., between 2 and 4 s) phases had similar flow field characteristics. However, slight differences were observed in the pharinx-larynx and bronchial regions at higher flow rates. Therefore, it can be inferred that when the peak value of inhalation flow rate increased from 15 L/min to 60 L/min, negligible differences in the distribution of flow rates were observed, which were not shown here. Consequently, the results were considered only at 1.5 and 3.5 s for the inhalation and the exhalation phase, respectively.

Fig. 6 depicts the velocity profiles on various cross-sectional regions indicated in Fig. 1 along the diametric direction for the flow rate of 30 L/min. The velocity distributions of different inhalation flow rates had a similar trend, but were not the same due to differing Re numbers (not shown in here). Herein, the velocity in each region was highly asymmetrical owing to the complexity of lung geometry. From the result of

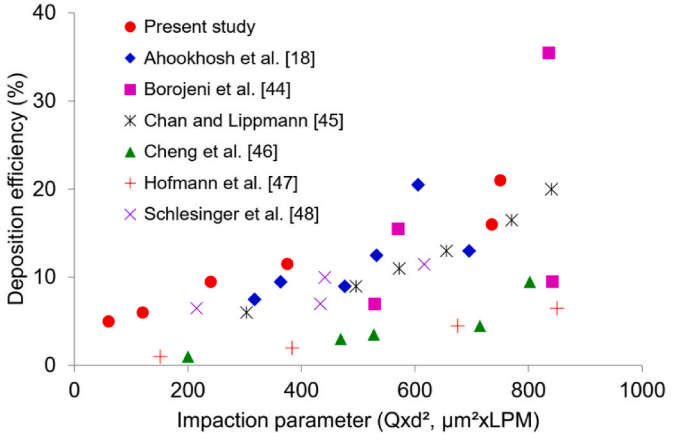

Fig. 5. Comparison of particle deposition efficiency reported in previous studies with the current study.

the simulation, it was determined that the highest velocity magnitude in the tracheal region was ~2.6 m/s. As air passed through any bifurcation region, the velocity distribution in each branch became highly irregular, as illustrated in Fig. 6d. These regions had higher local velocity profiles compared to the trachea, which was attributed to interactions between the inertial forces, the boundary layer effects, and the centrifugal forces at the curved bifurcations due to constricted airflow. As shown in Fig. 6c, the axial velocity increased to 4 m/s due to the reduction of bronchial lumen area.

Fig. 7 shows the velocity profiles in different segments during the inhalation and exhalation phase of the breathing cycle at the circulatory flow rate of 15 L/min. Compared with the results of our previous work [25], the circulatory breathing generally exhibited similar flow field characteristics to steady-state breathing at a specific moment. Due to the centrifugal forces, the velocity in the rear side of the extrathoracic region was greater than that in the front side, as shown in Fig. 7a and b. As the air flowed through the larynx, it accelerated and formed a recirculation pattern in the extrathoracic region, creating a flow separation region in the upper tracheal zone. This phenomenon, known as the laryngeal jet, significantly influences aerosol particle transport and deposition [10,18,25,33]. The air then flowed towards the trachea, the velocity distribution became more uniform (see Fig. 7c and d). Another feature observed in Fig. 7 after air passed through the bifurcation areas, the air velocity was increased on the inner airway walls facing the incoming flow while decreasing on the other side locally. Thus, it exhibited a very irregular flow pattern due to the complex geometry of the airways. In addition, the streamlines contracted in the flow separation regions, leading to an approximately 80 % increase in velocity. These velocity distributions are consistent with findings in the literature [4,14,18,26,33,49].

During the inhalation phase, the air developed throughout its flow and the velocity contours became like each other as it traveled deeper into the trachea. The tracheal area displayed a more uniform distribution of momentum (see Fig. 7c). However, upon entering the right and left bronchi, the air exhibited different flow velocities along the radial and flow directions. Due to the morphology of the bronchus, the velocity contours were non-uniform and a flow separation was also observed. Moreover, the right main bronchus was larger in diameter than the left main bronchus and deviated from the trachea at a smaller angle. Due to this asymmetry in the airway structure, the right lung was ventilated more.

During the exhalation phase, many different flow characteristics were observed, such as different flow patterns in the trachea, the formation of a jet due to a sudden decrease in velocity in the pharynx, and flow separation zones with smaller areas, as seen in Fig. 7b and d. The high flow velocities were observed in the front wall of the trachea during inspiration and in the center of the trachea during exhalation. With the upward motion of the flow during exhalation, the air from the bronchus merged into the trachea and a higher-velocity jet was formed. This effect became more prominent as the inhalation flow rate increased. In addition, the change in flow direction caused the formation of numerous vortices in the bronchial region. A more in-depth exploration of how the exhalation and inhalation phases distinct flow field properties affect particle deposition was offered in the following sections.

Figs. 8 and 9 show the velocity contours during the breathing cycle at circulatory inhalation flow rate of 30 and 60 L/min, respectively. The flow trends mentioned above were also observed here. Since the airway geometry was the main parameter for the fluid flow, the airflow patterns were generally similar at different inhalation flow rates throughout the model. The increase in the inhalation flow rate led to increase the airflow velocity. The flow separation exhibited minimal change, while the flow rate increased.

3.3. Particle distribution characteristics

Examining the distribution models of aerosol particles with different

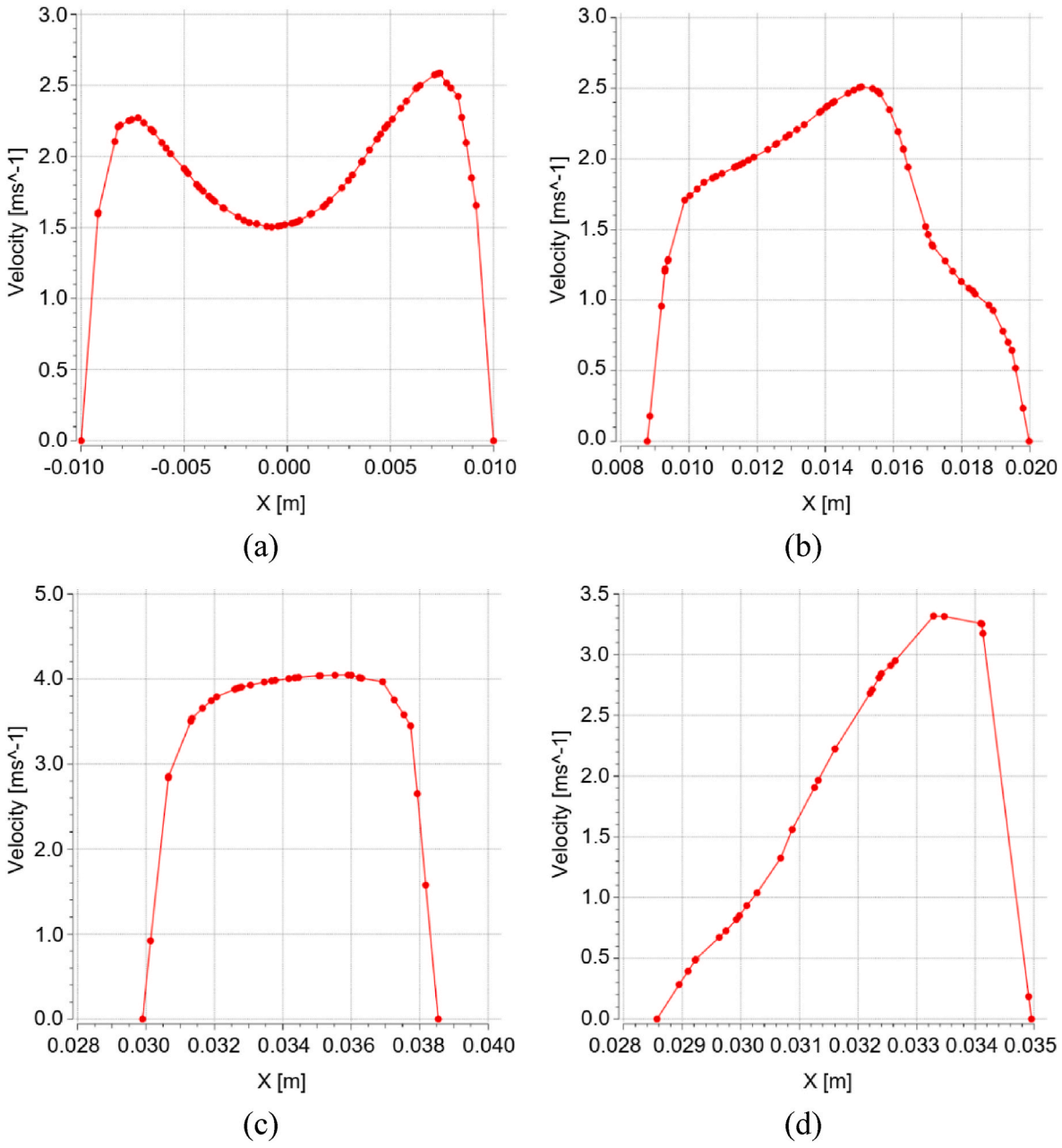

Fig. 6. The velocity profiles on different cross-sectional regions for the flow rate of 30 L/min at (a) Line 1, (b) Line 2, (c) Line 3, and (d) Line 4.

sizes used in the treatment of lung diseases is crucial for treatment success. A targeted aerosol drug delivery should be evaluated by considering the regional deposition under the realistic breathing conditions in the human airways. Therefore, determining the deposition of aerosol particles in the different regions of the respiratory system is very important in terms of treating diseases with the use of aerosol particles or assessing high-risk areas in case of exposure to polluted air. Moreover, it is very important to determine how particle deposition changes under more realistic breathing conditions. The deposition mechanisms of inhaled aerosol particles in the respiratory system are complicated because of their complex structure. Typically, the particle deposition in the respiratory tract is affected by breathing pattern and the particle size. The main deposition mechanism for the micro particles under light or normal breathing conditions is the gravitational sedimentation, while the inertial impaction is the primary mechanism for heavy activity [4, 10]. Particularly, the secondary airflow structures cause the deposition by impaction of inhaled aerosol particles on the respiratory tract walls [13,50].

One of the crucial parameters for drug delivery in the human airways is the distribution fraction, which refers to the ratio of deposited particles to the total inhaled in a given region. In this study, it was presented to evaluate the behavior of the aerosol particles. For the circulatory breathing condition, the aerosol particles suspended in the current airway zone at the end of the inhalation phase entered the previous zone by following the airflow during the exhalation phase. Fig. 10 shows the variation of the distribution fractions of 2, 5 and 7 μm particle sizes for different breathing conditions in different segments of the airway model, including extrathoracic, trachea, carina, bronchial tree (right and left bronchus). It is evident that the distribution fraction was significantly affected by the flow rate and the diameter of particle, with inertial impaction being the main factor controlling deposition. As seen in Fig. 10, most aerosol particles were distributed in the extrathoracic and bronchial region, while least deposited in the tracheal region. This is because the trachea is a long vertical straight airway without bending or

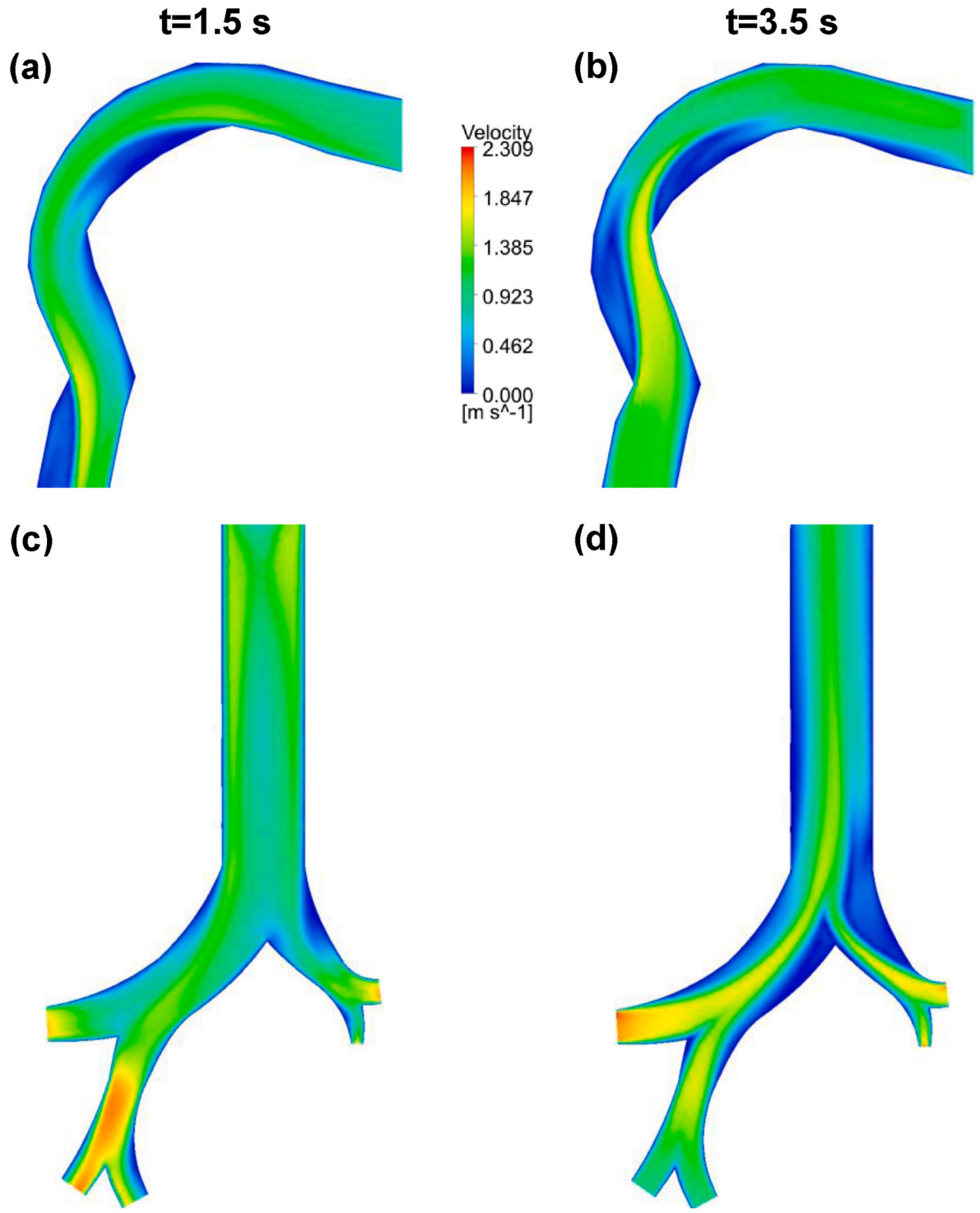

Fig. 7. The velocity contours on extrathoracic region (a and b), and trachea and bronchus region (c and d) at times of 1.5 and 3.5 s in the breathing cycle at inhalation flow rate of 15 L/min.

bifurcation, and hence the impaction is weak. At lower inhalation flow rates, a greater distribution fraction was observed for 2 μm particles in the bronchial tree compared with the extrathoracic region because the laminar flow dominated (see Fig. 10d). This phenomenon may be explained by the dimensionless Stokes number (St), which indicates how well a particle can follow the streamlines, and defined as:

$$St = \frac{\rho_p d_p^2 U}{18 \mu D} \tag{10}$$

where ρ_p is the particle density, d_p is the particle diameter, U is the mean velocity of the airflow, μ is the dynamic viscosity of air, and D is the airway diameter. In the case of a high St number, the particles cannot follow the liquid flow properly. Indeed, the complex structure of the extrathoracic and the bronchial region significantly deviating from the trachea will significantly alter the flow pattern. Since St number is proportional to both the flow velocity and the particle size, the increase in flow rate and particle size enhance St number, and therefore, the particles may not follow the streamlines and the particle-particle

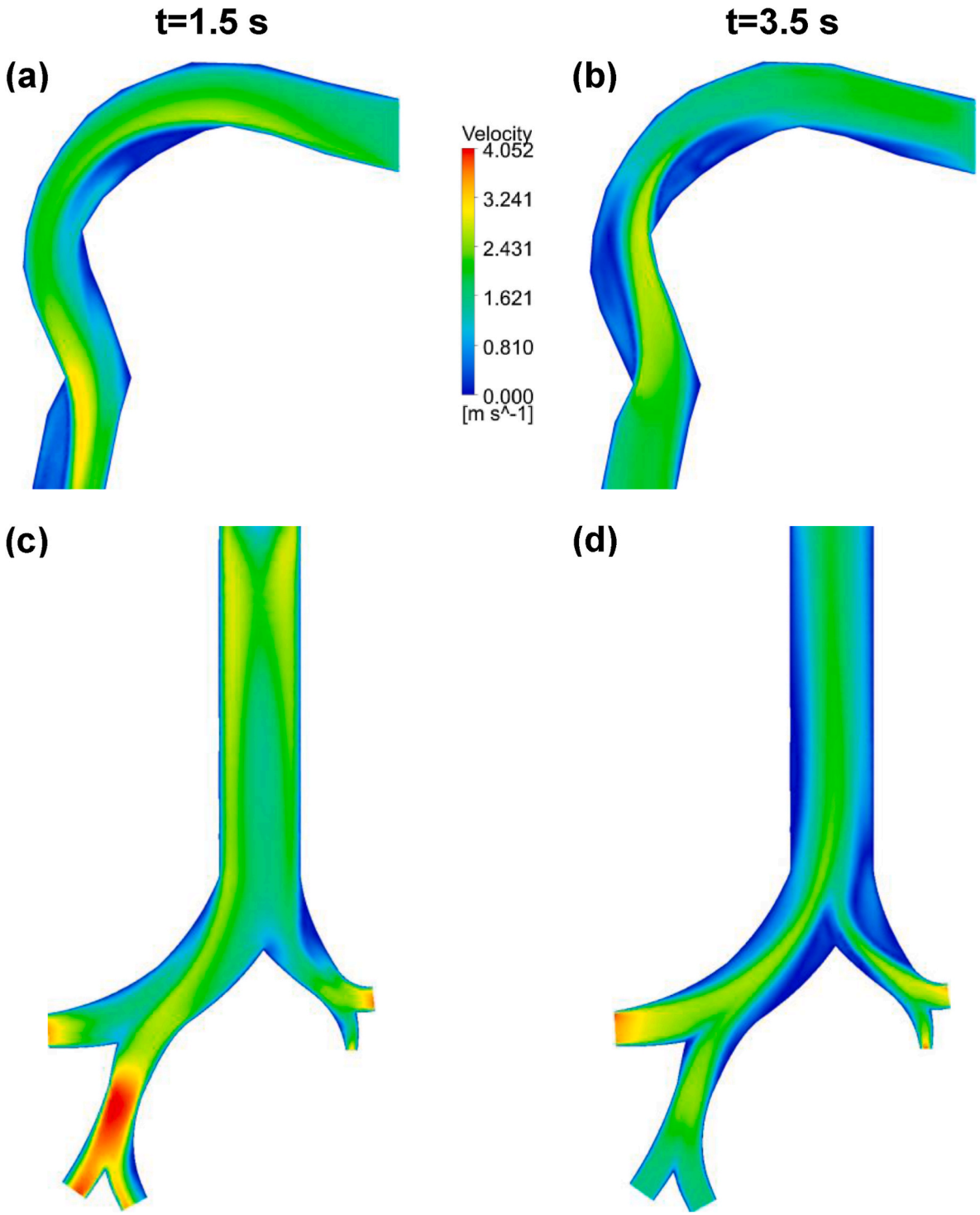

Fig. 8. The velocity contours on extrathoracic region (a and b), and trachea and bronchus region (c and d) at times of 1.5 and 3.5 s in the breathing cycle at a circulatory flow rate of 30 L/min.

interaction intensifies. On the contrary, as the flow rate decreases, the inertial effect weakens, which means a lower Stokes number. In this case, the aerosol particles move deep into the lung without hitting the airway inner walls. However, when the flow rate increases, the Stokes number also increases, and the stronger inertial impaction effect increases the deposition of particle in the extrathoracic region, while it decreases in other regions. Additionally, as the particle size increased, the inertia effect increased, and therefore, more 7 μm particles deposited in the extrathoracic zone. This effect became more evident with the increase in the flow rate (see Fig. 10a). As a result, in the case of a flow rate of 60 L/min with 7 μm particles, approximately 80 % particle deposition was found in the extrathoracic region.

Fig. 10 also showed that all particles exhibited similar distribution fractions for both constant and circulatory breathing conditions in the trachea and carina regions. Additionally, the same distribution fractions were found for 2 and 5 μm particles in the extrathoracic region. However, 7 μm particles exhibited slightly higher distribution fraction for the circulatory breathing with increasing flow rate. In the bronchial region,

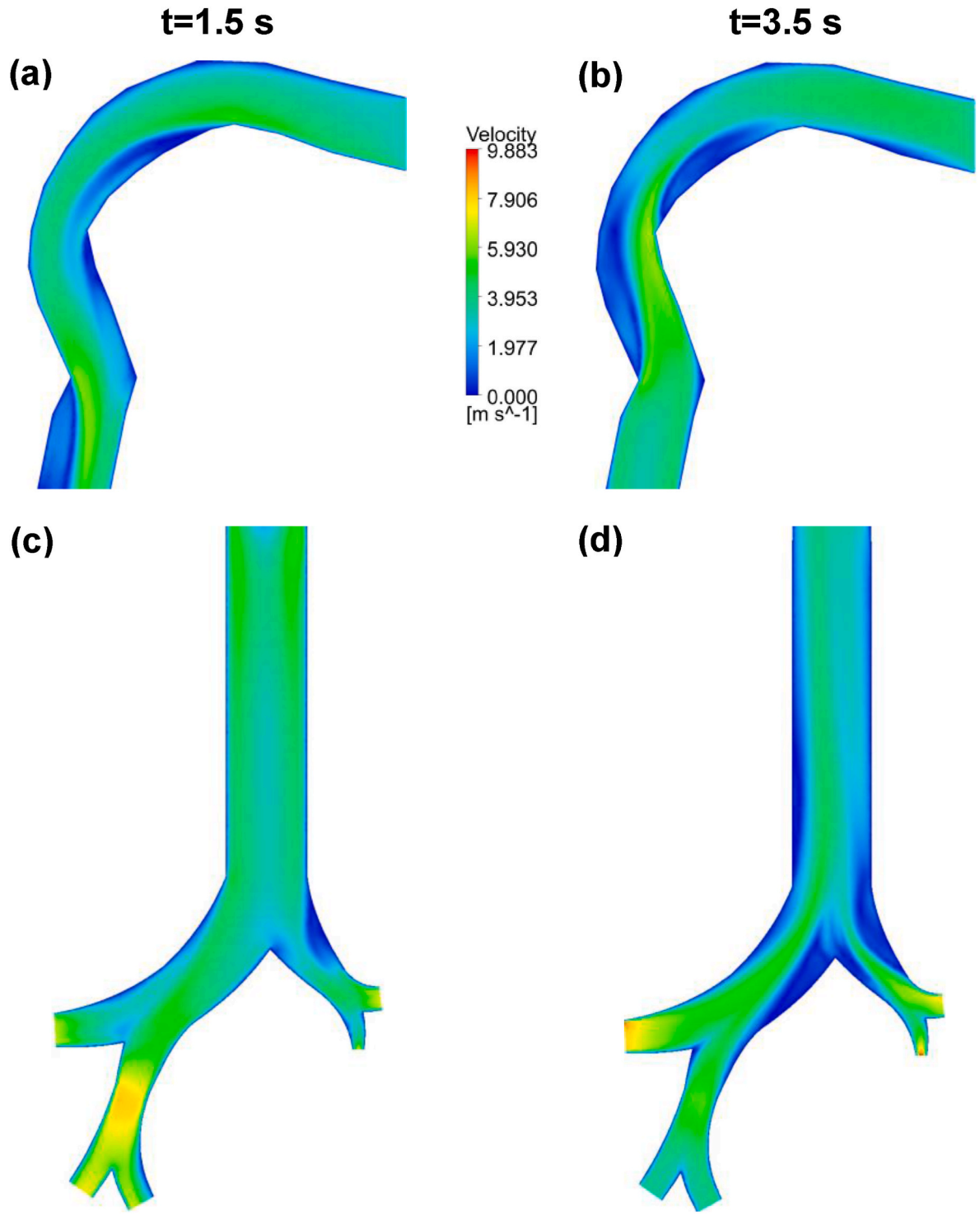

Fig. 9. The velocity contours on extrathoracic region (a and b), and trachea and bronchus region (c and d) at times of 1.5 and 3.5 s in the breathing cycle at a circulatory flow rate of 60 L/min.

slightly higher distribution fractions were found under the circulatory breathing condition for all particles. In circulatory breathing of 15 L/min, 2 μm particles deposited partly more in the extrathoracic region compared to the steady breathing, while they deposited less in other regions (see Fig. 10). This is because more particles are dispersed by the accelerated airflow during the inhalation phase and the particles come back to the extrathoracic region during the exhalation phase. For 7 μm particles and the flow rate of 15 L/min, a similar distribution fraction was found in the bronchial region in both breathing conditions (see Fig. 10d). When the flow rate exceeded to 15 L/min, there was a higher particle fractions in the bronchial zone for the circulatory breathing, especially for 7 μm particles. Thus, most particles with 7 μm in dimeter deposited in the bronchial and tracheal regions before reaching the extrathoracic region during exhalation. As a result, for effective treatment of bronchial diseases, especially for 2 μm particles, it is advisable to employ deep breathing under nearly constant respiratory conditions. This approach helps minimize the particle escape during the exhalation phase. Hence, inhaling smaller particles at lower velocities might be

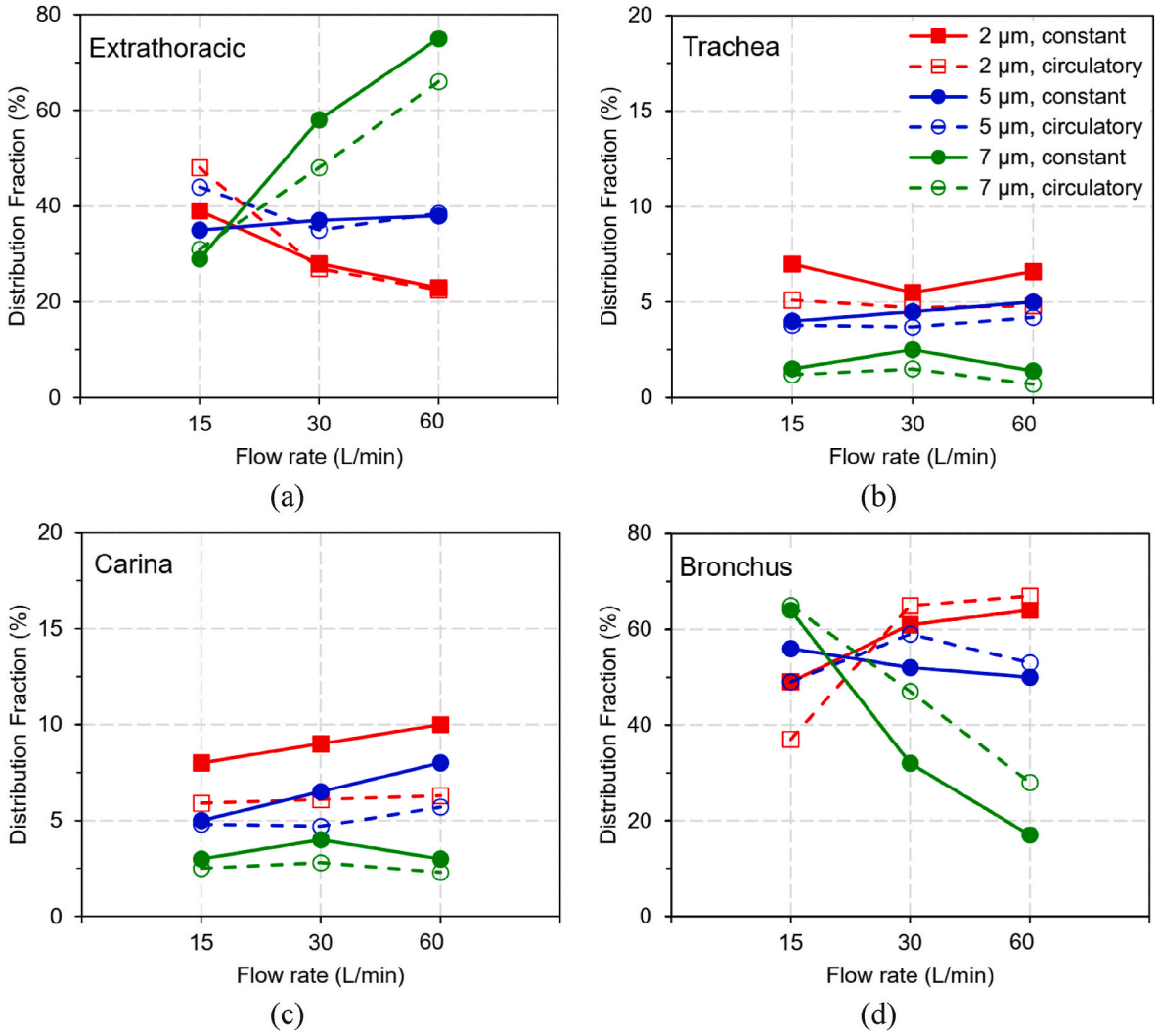

Fig. 10. The variation of the distribution fractions of 2, 5 and 7 μm particle sizes for different breathing conditions in different segments of the airway model. (a) Extrathoracic airways, (b) Trachea, (c) Carina, and (d) Bronchial tree.

recommended for patients having bronchial diseases.

Fig. 11 shows the non-uniform particle distribution in the right and left bronchus for 5 μm particles. For both the constant and circulatory breathing conditions, more particle deposition was observed in the right main bronchus, while less particle deposition was determined in the left main bronchus. This is because the flow rate in the right bronchus is higher and the separation angle of the right bronchus from the trachea is smaller. Similar trend was also observed for the other aerosol particles.

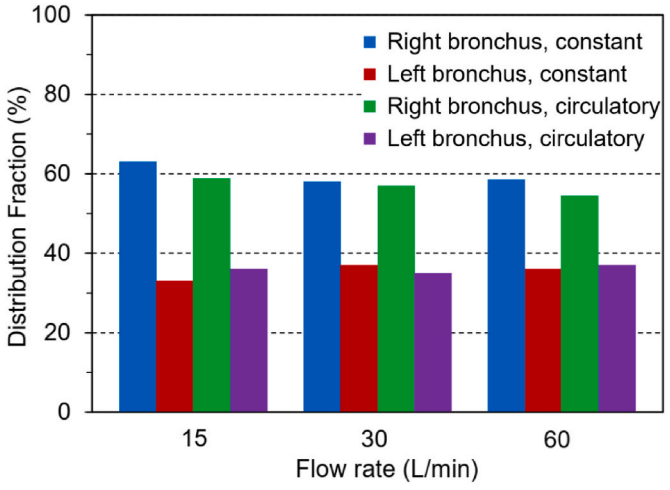

Fig. 11. The variation of the distribution fractions of 5 μm particles in the bronchial region.

The distributions of deposited particles in the human airway model were visually presented in Fig. 12. When the inhalation flow rate increased, the particle distribution grew up in the extrathoracic region while it reduced on trachea, especially for large particles. This is an undesirable situation in the effective treatment of respiratory diseases. As seen in Fig. 12, large particles were deposited more in the extrathoracic region than small particles due to its irregular and complex structure. This proves the theory that the impact mechanism becomes stronger as the particle diameter increases [50]. On the other hand, the right main bronchus was larger in diameter than the left main bronchus and deviated from the trachea at a smaller angle, leading to more ventilation, as mentioned above. Therefore, more particles occupied the right bronchus, resulting in greater particle deposition there, as shown in Fig. 12. This may be because the flow rate of the right bronchus is higher than that of the left bronchus, as denoted in the study of Ahookhosh et al. [27]. As a result, the number of particles dispersed deep into the lung from the right and left bronchus decreased with increasing the particle diameter.

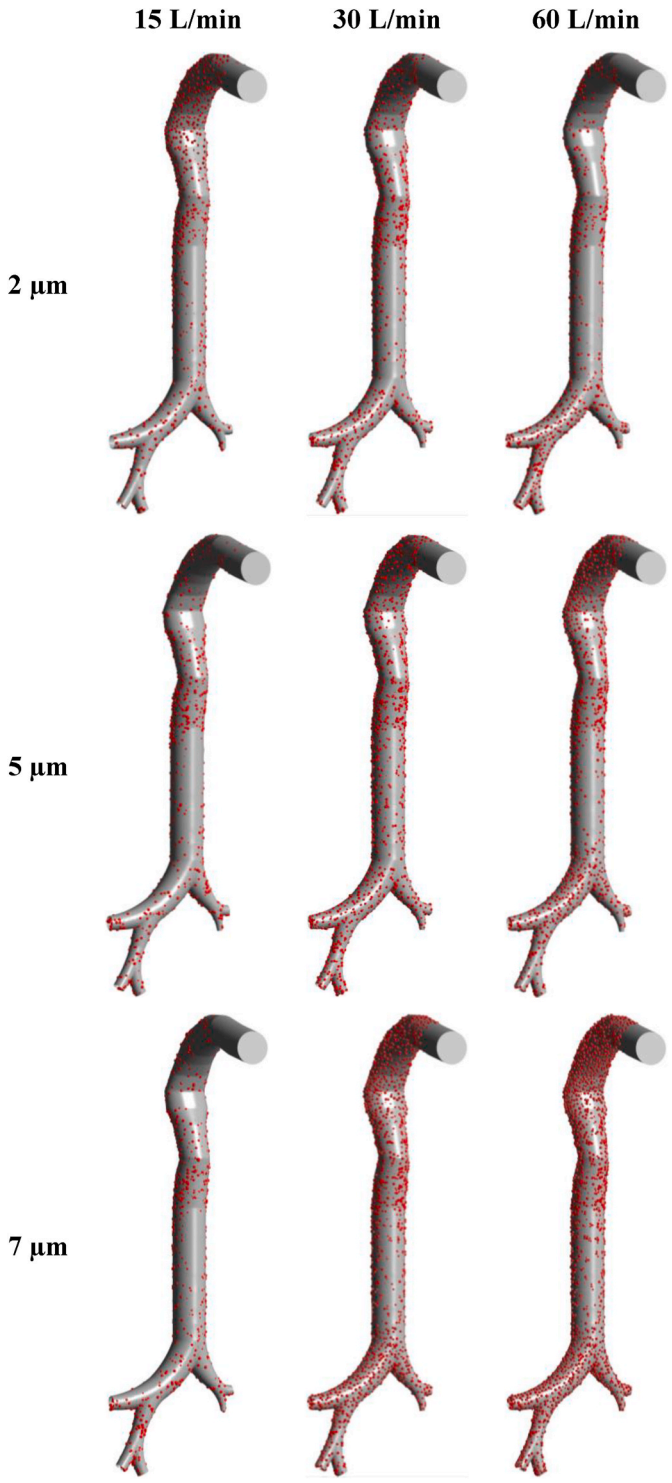

Fig. 12. The distribution of deposited particles in human airway walls under three different circulatory flow rates.

3.4. Particle deposition characteristics

Another important parameter for aerosol therapy and to risk assessment of air pollutants in the human airways is the deposition efficiency (η_d). In Fig. 13, the variation of η_d were compared for two breathing patterns at different flow rates. As seen, the particle size and the breathing flow rate significantly affected the drug delivery into the different segments. For example, in the extrathoracic region, the η_d of particles with $d_p = 2$ μm at flow rate of 60 L/min were significantly reduced compared to those at the flow rate of 15 L/min. As the flow rates increased, high air velocity forced the particles to follow the streamlines and weakened their impaction effects [50], resulting in lower η_d. Additionally, since the sedimentation effect of 2 μm particles was weaker, they were deposited less than large particles on the walls of the extrathoracic airways, as the flow rate increased. Moreover, during inhalation, reversal flows may occur in the bronchial region, which affect the particle deposition pattern in the airways. As a result, when the particle size decreases, they follow to the outlet instead of depositing on the inner walls of the airway model, exceeding the bifurcation areas and going deeper into the lung due to their inertial forces. In the tracheal region, on the other hand, the η_d value dropped because impaction was weak in straight airways, as mentioned in Section 3.3. In carina, on the contrary, the particle deposition increased with increasing the particle diameter and flow rate. Large particles struggle to follow the streamlines, resulting in reduced particle distribution in these regions. This outcome is aligned with the reported in the previous studies [33,37,49].

In the bronchial region, the decrease in airway diameter caused a decrease in flow rates towards the left bronchus and an increase in flow rates towards the right bronchus, as mentioned before. As shown in Fig. 13 for 2 μm particles and the flow rate of 15 L/min, lower η_d values were found because the laminar flow was predominant, and therefore, the small particles could reach deep into the lung. However, when the flow rates increased, the η_d increased significantly for large particles (5 and 7 μm) because of the strong inertial effect and sedimentation effect in this region [4,10,14,50]. A change in the direction of streamlines at high flow rates (i.e., the centrifugal effects) can increase the effect of inertial impact. Where the high-speed streamlines change the direction of large particles, the inertial effect forces them to follow their own tracks rather than follow the streamlines, so they collide with the airway walls, resulting in more particle deposition. This is known as deposition by typical impact mechanism. In the bronchial region, the Stokes number was larger due to the high flow velocities and the narrow air channels, resulting in a higher η_d value, as seen in Fig. 13. Additionally, similar to the distribution fraction, the η_d was also higher in the right lung than in the left lung. This implies that when the delivery of drugs is intended for the initial few generations of the lungs, high flow rates and large particles should be avoided. In other words, the particle size must be reduced to increase the number of particles escaping deep into the lung, resulting in the effective treatment of lung diseases. Consequently, this finding becomes crucial when aiming to precisely transport pharmaceutical particles to the target location in aerosol therapy. The numerical results presented here on the variation of total η_d with the aerosol particle diameter showed a good agreement with the literature results [25,30,51].

In Fig. 13, the η_d for circulatory breathing was observed to be elevated in the extrathoracic region but notably lower in the right and left bronchus compared to the constant breathing condition. This difference arises from the transportation of numerous particles suspended in the airways during the exhalation phase to the extrathoracic region. 7 μm particles tended to deposit especially in the rear side of the extrathoracic region due to their high speed and larger inertia. Thus, at the flow rates of 30 and 60 L/min, they had higher η_d values in all regions under constant breathing condition. Additionally, the breathing flow velocity was lower under the circulatory breathing than the constant breathing, resulting in more particles being released from the extrathoracic region. Detailed examination of regional deposition would aid in the development of targeted aerosol drug delivery methods.

According to the results obtained in this study, the particle deposition efficiencies increased with the flow rate and the particle size. In these conditions, the majority of particles deposited in the extrathoracic region before reaching the bronchial region. For this reason, it is advisable to avoid selecting a high inhalation flow rate for the effective treatment of bronchial diseases. The results also indicated that both the particle deposition efficiency and the distribution fraction were higher in the right lung compared to the left lung. Thus, it can be said that the

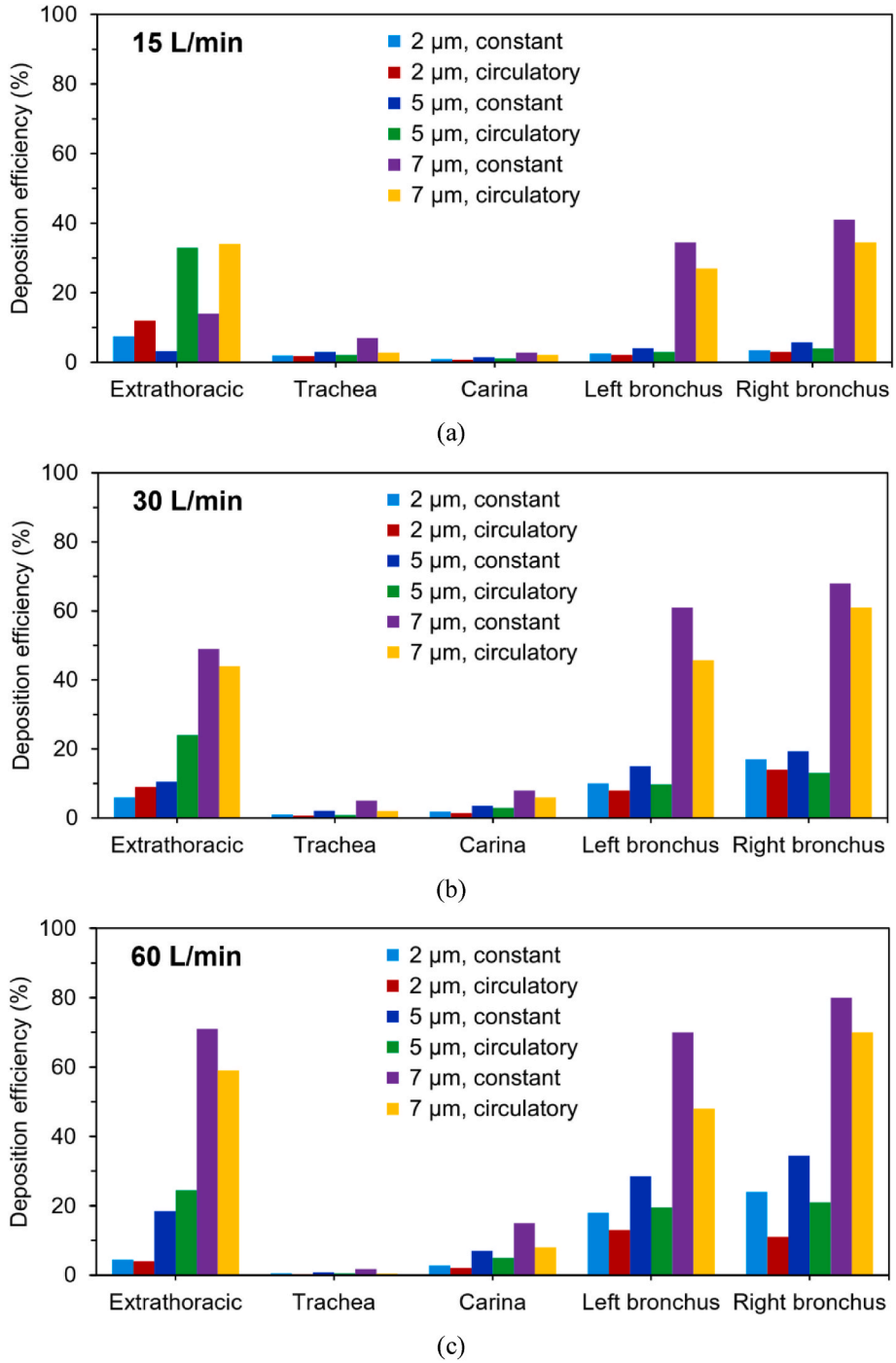

Fig. 13. The particle deposition efficiencies in the different segments of the human airway model under different constant and circulatory respiratory flow rates. (a) 15 L/min, (b) 30 L/min, and (c) 60 L/min.

right lung will absorb more drugs and be more effective in treating the diseases. For the treatment of the left lung diseases, the inhalation flow rate should be increased appropriately. However, it should not be forgotten that this situation can increase a possible health risk by inhaling pollutants in the air.

4. Conclusion

In this study, the regional depositions of the aerosol particles were numerically examined in a CT based model of the human airway including the mouth-throat area and the tracheobronchial upper respiratory tract. In the simulations, a k-ω turbulence model was used to represent the transitional airflow characteristics. A Lagrangian approach was also employed to track the trajectories of aerosol particles and simulate their deposition in the flow field. Three different circulatory breathing conditions for people under light, normal, and heavy physical activities were applied, and aerosol particles with diameters of 2, 5, and 7 μm were injected into the mouth, considering oral inhalation. The numerical results showed that the airflow was characteristically similar for both the constant and the circulatory breathing conditions. On the other hand, most aerosol particles were deposited in the extrathoracic and bronchial region. When the inhalation flow rate increased, 2 μm particles moved specifically towards the bronchial region and were delivered to the deep lung, while larger particles deposited especially in

the extrathoracic region. In the trachea and carina regions for both breathing conditions, the particles exhibited almost the same distribution fraction. Additionally, the same distribution fractions were found for 2 and 5 μm particles in the extrathoracic region. In the extrathoracic region, however, 7 μm particles exhibited slightly higher distribution fraction for the circulatory breathing with increasing flow rate. As the aerosol particle size and flow rate increased, the distribution fraction of the particles for circulatory breathing was slightly higher than under constant breathing condition in the bronchial region for all particles. Typically, more particles deposited in the right bronchus than in the left bronchus, regardless of breathing condition. The results presented here also indicated that the deposition efficiency for circulatory breathing was high in the extrathoracic region but significantly lower in the bronchial region compared to the constant breathing condition. The particle sizes and flow rates used in this study are very similar to the device data provided by dry powder inhalers (DPIs) [52–56]. Therefore, the use of DPIs can be recommended for treatment as they are chemically stable, easily transportable, easy to use and cost-effective.

The limitations of this study include consideration of a limited number of bronchial airway generations, rigidity of the model walls, assumption of one-way coupling, assumption of sinusoidal flow profile, assumption of simple 0 Pa outlet pressure, assumption that particles do not return during exhalation, neglect of the mouthpiece effect of an inhalation device, and the possibility that the numerical results were not validated by experimental data. In the future, the study could be expanded to include these limitations. Therefore, although the proposed analysis may help improve clinical drug-aerosol targeting and understand microparticle deposition in airway geometry, the presented results should be treated with caution and generalized throughout several different airway models. The results can essentially form the basis for further experimental and numerical studies.

CRediT authorship contribution statement

Dogan Ciloglu: Writing – review & editing, Writing – original draft, Validation, Methodology, Investigation.

Declaration of competing interest

The author declares no conflict of interest.

Data availability

Data will be made available on request.

Acknowledgments

This research was supported by the FAB-2021-9407 project of the Research Fund of Ataturk University. The author thanks Prof. Dr. Adem Karaman for providing the CT-scan image of the subject's respiratory tract.

References

[1] A.M. Healy, M.I. Amaro, K.J. Paluch, L. Tajber, Dry powders for oral inhalation free of lactose carrier particles, Adv. Drug Deliv. Rev. 75 (2014) 32–52, https://doi.org/10.1016/j.addr.2014.04.005.
[2] D.-K. Ho, B.L.B. Nichols, K.J. Edgar, X. Murgia, B. Loretz, C.-M. Lehr, Challenges and strategies in drug delivery systems for treatment of pulmonary infections, Eur. J. Pharm. Biopharm. 144 (2019) 110–124, https://doi.org/10.1016/j.ejpb.2019.09.002.
[3] M.H. Taheri, O. Pourmehran, M.M. Sarafraz, K. Ahookhosh, A. Farnoud, X. Cui, Effect of swirling flow and particle-release pattern on drug delivery to human tracheobronchial airways, Biomech. Model. Mechanobiol. 20 (2021) 2451–2469, https://doi.org/10.1007/s10237-021-01518-5.
[4] C. Kleinstreuer, Z. Zhang, Z. Li, Modeling airflow and particle transport/deposition in pulmonary airways, Respir. Physiol. Neurobiol. 163 (2008) 128–138, https://doi.org/10.1016/j.resp.2008.07.002.
[5] M. Rahimi-Gorji, C. Debbaut, G. Ghorbaniasl, S. Cosyns, W. Willaert, W. Ceelen, Optimization of intraperitoneal aerosolized drug delivery using computational fluid dynamics (CFD) modeling, Sci. Rep. 12 (2022) 6305, https://doi.org/10.1038/s41598-022-10369-8.
[6] M. Tullio, L. Aliboni, F. Pennati, R. Carrinola, A. Palleschi, A. Aliverti, Computational fluid dynamics of the airways after left-upper pulmonary lobectomy: a case study, Int J Numer Method Biomed Eng 37 (2021) 1–18, https://doi.org/10.1002/cnm.3462.
[7] J. Kim, R.M. Pidaparti, Computational analysis of lung and isolated airway bifurcations under mechanical ventilation and normal breathing, Fluid 6 (2021) 388, https://doi.org/10.3390/fluids6110388.
[8] D. Ciloglu, A numerical study of the aerosol behavior in intra-acinar region of a human lung, Phys. Fluids 32 (2020) 103305, https://doi.org/10.1063/5.0024200.
[9] D. Ciloglu, Numerical simulation of the unsteady flow field in the human pulmonary acinus, Sādhanā 46 (2021) 186, https://doi.org/10.1007/s12046-021-01704-2.
[10] Z. Zhang, C. Kleinstreuer, Airflow structures and nano-particle deposition in a human upper airway model, J. Comput. Phys. 198 (2004) 178–210, https://doi.org/10.1016/j.jcp.2003.11.034.
[11] M. Rahimi-Gorji, L. Van de Sande, C. Debbaut, G. Ghorbaniasl, H. Braet, S. Cosyns, K. Remaut, W. Willaert, W. Ceelen, Intraperitoneal aerosolized drug delivery: technology, recent developments, and future outlook, Adv. Drug Deliv. Rev. 160 (2020) 105–114, https://doi.org/10.1016/j.addr.2020.10.015.
[12] S. Tanprasert, C. Kampeewichean, S. Shiratori, R. Piemjaiswang, B. Chalermsinsuwan, Non-spherical drug particle deposition in human airway using computational fluid dynamics and discrete element method, Int. J. Pharm. 639 (2023) 122979, https://doi.org/10.1016/j.ijpharm.2023.122979.
[13] P.W. Longest, S. Vinchurkar, Inertial deposition of aerosols in bifurcating models during steady expiratory flow, J. Aerosol Sci. 40 (2009) 370–378, https://doi.org/10.1016/j.jaerosci.2008.11.007.
[14] M. Malvè, C. Sánchez-Matás, J.L. López-Villalobos, Modelling particle transport and deposition in the human healthy and stented tracheobronchial airways, Ann. Biomed. Eng. 48 (2020) 1805–1820, https://doi.org/10.1007/s10439-020-02493-1.
[15] H. Braet, M. Rahimi-Gorji, C. Debbaut, G. Ghorbaniasl, T. Van Walleghem, S. Cornelis, S. Cosyns, C. Vervaet, W. Willaert, W. Ceelen, S.C. De Smedt, K. Remaut, Exploring high pressure nebulization of Pluronic F127 hydrogels for intraperitoneal drug delivery, Eur. J. Pharm. Biopharm. 169 (2021) 134–143, https://doi.org/10.1016/j.ejpb.2021.10.001.
[16] M. Rahimi-Gorji, T.B. Gorji, M. Gorji-Bandpy, Details of regional particle deposition and airflow structures in a realistic model of human tracheobronchial airways: two-phase flow simulation, Comput. Biol. Med. 74 (2016) 1–17, https://doi.org/10.1016/j.compbiomed.2016.04.017.
[17] Z. Zhang, C. Kleinstreuer, C.S. Kim, Computational analysis of micron-particle deposition in a human triple bifurcation airway model, Comput. Methods Biomech. Biomed. Eng. 5 (2002) 135–147, https://doi.org/10.1080/10255840290032153.
[18] K. Ahookhosh, S. Yaqoubi, M. Mohammadpourfard, H. Hamishehkar, H. Aminfar, Experimental investigation of aerosol deposition through a realistic respiratory airway replica: an evaluation for MDI and DPI performance, Int. J. Pharm. 566 (2019) 157–172, https://doi.org/10.1016/j.ijpharm.2019.05.058.
[19] K. Inthavong, K. Zhang, J. Tu, Numerical modelling of nanoparticle deposition in the nasal cavity and the tracheobronchial airway, Comput. Methods Biomech. Biomed. Eng. 14 (2011) 633–643, https://doi.org/10.1080/10255842.2010.493510.
[20] R. Ravi Kannan, A.J. Przekwas, N. Singh, R. Delvadia, G. Tian, R. Walenga, Pharmaceutical aerosols deposition patterns from a Dry Powder Inhaler: euler Lagrangian prediction and validation, Med. Eng. Phys. 42 (2017) 35–47, https://doi.org/10.1016/j.medengphy.2016.11.007.
[21] E.R. Weibel, Morphometry of the Human Lung, Springer Berlin Heidelberg, Berlin, Heidelberg, 1963, https://doi.org/10.1007/978-3-642-87553-3.
[22] J. Fleming, J. Conway, C. Majoral, L. Tossici-Bolt, I. Katz, G. Caillibotte, D. Perchet, M. Pichelin, B. Muellinger, T. Martonen, P. Kroneberg, G. Apiou-Sbirlea, The use of combined single photon emission computed tomography and X-ray computed tomography to assess the fate of inhaled aerosol, J. Aerosol Med. Pulm. Drug Deliv. 24 (2011) 49–60, https://doi.org/10.1089/jamp.2010.0843.
[23] L. Golshahi, M.L. Noga, R.B. Thompson, W.H. Finlay, In vitro deposition measurement of inhaled micrometer-sized particles in extrathoracic airways of children and adolescents during nose breathing, J. Aerosol Sci. 42 (2011) 474–488, https://doi.org/10.1016/j.jaerosci.2011.04.002.
[24] M. Rahimi-Gorji, O. Pourmehran, M. Gorji-Bandpy, T.B. Gorji, CFD simulation of airflow behavior and particle transport and deposition in different breathing conditions through the realistic model of human airways, J. Mol. Liq. 209 (2015) 121–133, https://doi.org/10.1016/j.molliq.2015.05.031.
[25] D. Ciloglu, A. Karaman, A numerical simulation of the airflow and aerosol particle deposition in a realistic airway model of a healthy adult, J. Pharmaceut. Sci. 111 (2022) 3130–3140, https://doi.org/10.1016/j.xphs.2022.08.005.
[26] K. Poorbahrami, J.M. Oakes, Regional flow and deposition variability in adult female lungs: a numerical simulation pilot study, Clin. BioMech. 66 (2019) 40–49, https://doi.org/10.1016/j.clinbiomech.2017.12.014.
[27] K. Ahookhosh, M. Saidi, M. Mohammadpourfard, H. Aminfar, H. Hamishehkar, A. Farnoud, O. Schmid, Flow structure and particle deposition analyses for optimization of a pressurized metered dose inhaler (pMDI) in a model of tracheobronchial airway, Eur. J. Pharmaceut. Sci. 164 (2021) 105911, https://doi.org/10.1016/j.ejps.2021.105911.
[28] K. Ahookhosh, M. Saidi, H. Aminfar, M. Mohammadpourfard, H. Hamishehkar, S. Yaqoubi, Dry powder inhaler aerosol deposition in a model of tracheobronchial

airways: validating CFD predictions with in vitro data, Int. J. Pharm. 587 (2020) 119599, https://doi.org/10.1016/j.ijpharm.2020.119599.
[29] H. Calmet, G. Houzeaux, M. Vázquez, B. Eguzkitza, A.M. Gambaruto, A.J. Bates, D. J. Doorly, Flow features and micro-particle deposition in a human respiratory system during sniffing, J. Aerosol Sci. 123 (2018) 171–184, https://doi.org/10.1016/j.jaerosci.2018.05.008.
[30] P.G. Koullapis, L. Nicolaou, S.C. Kassinos, In silico assessment of mouth-throat effects on regional deposition in the upper tracheobronchial airways, J. Aerosol Sci. 117 (2018) 164–188, https://doi.org/10.1016/j.jaerosci.2017.12.001.
[31] Y. Ostrovski, S. Dorfman, M. Mezhericher, S. Kassinos, J. Sznitman, Targeted drug delivery to upper airways using a pulsed aerosol bolus and inhaled volume tracking method, Flow, Turbul. Combust. 102 (2019) 73–87, https://doi.org/10.1007/s10494-018-9927-1.
[32] X. Xu, J. Wu, W. Weng, M. Fu, Investigation of inhalation and exhalation flow pattern in a realistic human upper airway model by PIV experiments and CFD simulations, Biomech. Model. Mechanobiol. 19 (2020) 1679–1695, https://doi.org/10.1007/s10237-020-01299-3.
[33] A. Arsalanloo, M. Abbasalizadeh, M. Khalilian, Y. Saniee, A. Ramezanpour, M. S. Islam, A computational approach to understand the breathing dynamics and pharmaceutical aerosol transport in a realistic airways, Adv. Powder Technol. 33 (2022) 103635, https://doi.org/10.1016/j.apt.2022.103635.
[34] J. Wang, Y. Zhang, X. Chen, Y. Feng, X. Ren, M. Yang, T. Ding, Targeted delivery of inhalable drug particles in a patient-specific tracheobronchial tree with moderate COVID-19: a numerical study, Powder Technol. 405 (2022) 117520, https://doi.org/10.1016/j.powtec.2022.117520.
[35] F. Huang, Y. Zhang, Z.B. Tong, X.L. Chen, R.Y. Yang, A.B. Yu, Numerical investigation of deposition mechanism in three mouth–throat models, Powder Technol. 378 (2021) 724–735, https://doi.org/10.1016/j.powtec.2018.11.095.
[36] M.J. Oldham, Computational fluid dynamic predictions and experimental results for particle deposition in an airway model, Aerosol. Sci. Technol. 32 (2000) 61–71, https://doi.org/10.1080/027868200303939.
[37] H. Liu, S. Ma, T. Hu, D. Ma, Computational investigation of flow characteristics and particle deposition patterns in a realistic human airway model under different breathing conditions, Respir. Physiol. Neurobiol. 314 (2023) 104085, https://doi.org/10.1016/j.resp.2023.104085.
[38] C.-C. Chuang, J.K. Mutuku, C.-C. Chueh, A. Selvarajoo, W.-H. Chen, Fine particulate matter deposition in 3D out-of-plane bifurcation lung airway, Aerosol Air Qual. Res. 23 (2023) 220392, https://doi.org/10.4209/aaqr.220392.
[39] Z. Zhang, C. Kleinstreuer, C.S. Kim, Gas–solid two-phase flow in a triple bifurcation lung airway model, Int. J. Multiphas. Flow 28 (2002) 1021–1046, https://doi.org/10.1016/S0301-9322(02)00011-3.
[40] Y. Aghaei, B. Sajadi, G. Ahmadi, The effect of the mucus layer and the inhaled air conditions on the droplets fate in the human nasal cavity: a numerical study, J. Aerosol Sci. 171 (2023) 106163, https://doi.org/10.1016/j.jaerosci.2023.106163.
[41] H.L. Dailey, S.N. Ghadiali, Fluid-structure analysis of microparticle transport in deformable pulmonary alveoli, J. Aerosol Sci. 38 (2007) 269–288, https://doi.org/10.1016/j.jaerosci.2007.01.001.
[42] S.A. Morsi, A.J. Alexander, An investigation of particle trajectories in two-phase flow systems, J. Fluid Mech. 55 (1972) 193–208, https://doi.org/10.1017/S0022112072001806.
[43] M.S. Islam, S.C. Saha, T. Gemci, I.A. Yang, E. Sauret, Y.T. Gu, Polydisperse microparticle transport and deposition to the terminal bronchioles in a heterogeneous vasculature tree, Sci. Rep. 8 (2018) 16387, https://doi.org/10.1038/s41598-018-34804-x.
[44] A.A.T. Borojeni, M.L. Noga, R. Vehring, W.H. Finlay, Measurements of total aerosol deposition in intrathoracic conducting airway replicas of children, J. Aerosol Sci. 73 (2014) 39–47, https://doi.org/10.1016/j.jaerosci.2014.03.005.
[45] T.L. Chan, M. Lippmann, Experimental measurements and empirical modelling of the regional deposition of inhaled particles in humans, Am. Ind. Hyg. Assoc. J. 41 (1980) 399–409, https://doi.org/10.1080/15298668091424942.
[46] Y.-S. Cheng, Y. Zhou, B.T. Chen, Particle deposition in a cast of human oral airways, Aerosol. Sci. Technol. 31 (1999) 286–300, https://doi.org/10.1080/027868299304165.
[47] W. Hofmann, T.B. Martonen, R.C. Graham, Predicted deposition of nonhygroscopic aerosols in the human lung as a function of subject age, J. Aerosol Med. 2 (1989) 49–68, https://doi.org/10.1089/jam.1989.2.49.
[48] R.B. Schlesinger, D.E. Bohning, T.L. Chan, M. Lippmann, Particle deposition in a hollow cast of the human tracheobronchial tree, J. Aerosol Sci. 8 (1977) 429–445, https://doi.org/10.1016/0021-8502(77)90036-2.
[49] M. Rahman, M. Zhao, M.S. Islam, K. Dong, S.C. Saha, Numerical study of nano and micro pollutant particle transport and deposition in realistic human lung airways, Powder Technol. 402 (2022) 117364, https://doi.org/10.1016/j.powtec.2022.117364.
[50] C. Darquenne, Deposition mechanisms, J. Aerosol Med. Pulm. Drug Deliv. 33 (2020) 181–185, https://doi.org/10.1089/jamp.2020.29029.cd.
[51] C. Darquenne, M. Paiva, J.B. West, G.K. Prisk, Effect of microgravity and hypergravity on deposition of 0.5- to 3-μm-diameter aerosol in the human lung, J. Appl. Physiol. 83 (1997) 2029–2036, https://doi.org/10.1152/jappl.1997.83.6.2029.
[52] M.E.A.C. Broeders, J. Molema, N.A. Vermue, H. Th, M. Folgering, Peak inspiratory flow rate and slope of the inhalation profiles in dry powder inhalers, Eur. Respir. J. 18 (2001) 780–783, https://doi.org/10.1183/09031936.01.00240301.
[53] T. Srichana, G.P. Martin, C. Marriott, Dry powder inhalers: the influence of device resistance and powder formulation on drug and lactose deposition in vitro, Eur. J. Pharmaceut. Sci. 7 (1998) 73–80, https://doi.org/10.1016/S0928-0987(98)00008-6.
[54] X. Liu, D. Rua, A. Wokovich, C. Guo, D. Keire, Particle size distribution analysis of OTC aerosol or powder drug products with potential for inadvertent inhalation exposure to consumers, J. Pharmaceut. Sci. 108 (2019) 1506–1511, https://doi.org/10.1016/j.xphs.2018.10.066.
[55] J. Williams, J. Kolehmainen, S. Cunningham, A. Ozel, U. Wolfram, Image-based modelling of inhaler deposition during respiratory exacerbation, medRxiv (2020). https://api.semanticscholar.org/CorpusID:219544715.
[56] Y.L. de Charras, M.V. Ramírez-Rigo, D.E. Bertin, Prediction of the particle size distribution of the aerosol generated by a pressurized metered-dose inhaler, Powder Technol. 399 (2022) 117151, https://doi.org/10.1016/j.powtec.2022.117151.